Electronic ISSN: 1309-0267

International Journal of Engineering & Applied Sciences

IJEAS

I J E A S

Volume 14, Issue 3
2022

Published by Akdeniz University

Editorial Board

(The name listed below is not Alphabetical or any title scale)

Abstracting & Indexing

IJEAS provides unique **DOI** link to every paper published.

Editorial Scope

The journal presents its readers with broad coverage across some branches of engineering and science of the latest development and application of new solution algorithms, artificial intelligent techniques innovative numerical methods and/or solution techniques directed at the utilization of computational methods in solid and nano-scaled mechanics.

International Journal of Engineering & Applied Sciences (IJEAS) is an Open Access Journal

International Journal of Engineering & Applied Sciences (IJEAS) publish original contributions on the following topics:

Civil Engineering: numerical modelling of structures, seismic evaluation, experimental testing, construction and management, geotechnical engineering, water resources management, groundwater modelling, coastal zone modelling, offshore structures, water processes, desalination, waste-water treatment, pavement and maintenance, transport and traffic, laser scanning, and hydrographic surveying, numerical methods in solid mechanics, nanomechanic and applications, microelectromechanical systems (MEMS), vibration problems in engineering, higher order elasticity (strain gradient, couple stress, surface elasticity, nonlocal elasticity)

Electrical Engineering: artificial and machine intelligence and robotics, automatic control, bioinformatics and biomedical engineering, communications, computer engineering and networks, systems security and data encryption, electric power engineering and drives, embedded systems, Internet of Things (IoT), microwaves and optics.

Engineering Mathematics and Physics: computational and stochastic methods, optimization, nonlinear dynamics, modelling and simulation, computer science, solid state physics and electronics, computational electromagnetics, biophysics, atomic and molecular physics, thermodynamics, geophysical fluid dynamics, wave mechanics, and solid mechanics.

Mechanical Engineering: machine design, materials science, mechanics of materials, manufacturing engineering and technology, dynamics, robotics, control, industrial engineering, ergonomics, energy, combustion, heat transfer, fluids mechanics, thermodynamics, turbo machinery, aerospace research, aerodynamics, and propulsion.

CONTENTS

Numerical Analysis of Single Lap Pretension Bolted Joint

By Sena Sevinç, Melis Taşkın *77-90*

Probabilistic Seismic Hazard Analysis of Burdur City

By Mehmet Alpyürür *91-99*

International Journal of Engineering & Applied Sciences (IJEAS)
Vol.14, Issue 3 (2022) 77-90
http://dx.doi.org/10.24107/ijeas.1218294
Int J Eng Appl Sci 14(3) (2022) 77-90

Numerical Analysis of Single Lap Pretension Bolted Joint

Sena Sevinç, Melis Taşkın *

Süleyman Demirel University,Civil Engineering Department, Isparta, Turkey
**E-mail address*: melistskn@gmail.com *, senasevinc.096@gmail.com

ORCID numbers of author:
*0000-0001-6233-2244 , 0000-0002-7143-9382 **

Received date: 13.12.2022
Accepted date: 16.12.2022

Abstract

Due to their superiority, bolted connections are commonly utilized to join numerous building components. When evaluating the impacts of the connections on the behavior and load-bearing capacity of structural systems, it is crucial to understand the parameters that govern the load-carrying capacity of bolted joints. The bearing capacity of single lap and single bolt slip-critical joints are examined numerically in this paper. Through numerical analysis, the variation in the bearing capacity of the joint as a function of the parameters affecting joint capacity, the pre-tension force, and the surface friction coefficient between the joining plates, was analyzed. Accordingly, it has been observed that the pre-tensioning force and friction coefficient both increase the joint's capacity in a comparable manner. The results demonstrate that the bearing capacity of a slip-critical joint can be enhanced by applying roughening techniques to the friction surfaces of the plate.

Keywords: Single lap bolted joint, pretension load, friction coefficient, numerical analysis.

1. Introduction

It is known that a significant part of the damage to the structural elements under the loads they are exposed to is caused by the joints. For this reason, it is essential to design and analyze the joint areas correctly. There are different connection types in terms of material and application method. One of these, which has widespread usage, is bolted connections. Bolted connections have advantages such as application, material supply, standard features, mass production, ease of assembly, and economicalness.

In the Specification for the Design, Calculation, and Construction of Steel Structures (SDCCSS) joints are classified as bearing and slip-critical. Slip-critical joints are those in which the bolts are tightened by applying a pre-tensioning force and are formed in such a way as to prevent slipping between the contact surfaces of the joining parts. The pre-tension force applied using high-strength bolts in slip-critical joints is transferred by friction forces. In addition, the bolt shank's shear strength and the stress distribution around the hole are effective in load transfer [1].

The bearing capacity and failure of the joint vary depending on many parameters. It is known that these parameters are generally joint geometry, plate and bolt material, preload, and friction coefficient [2]. Therefore, the investigation of the bearing capacity of the joint has been a prevalent subject [3-6].

McCarthy et al. [7] investigated the effects of boundary conditions and hole clearance on the joint using finite element analysis. Saraç [8] numerically studied the effect of hole diameter and bolt tightening torque changes on the load-carrying capacity of a single-acting bolted joint. Numerical analysis showed that bolt-tightening torque is a more effective parameter in increasing the bearing capacity of the joint. Ghanbari et al. [9] investigated the variation of the behavior of single lap glass fiber reinforced epoxy (GFRE) composites under tension and simple bending according to bolt placement distances and tightening torque. As a result of the experimental study, the value of failure-bearing stress increased with the tightening torque.

Chakherlou and Jirandehi [10] investigated the effects of friction coefficients on different contact surfaces of a single-lap single-bolt joint using FEM. They found that increasing friction coefficients between the joining means and the plate reduces the compressive stresses around the hole. Khashaba et al. [11] experimentally investigated the effects of tightening torque and washer size parameters on the strength of glass fiber-reinforced epoxy composite bolted joints. It has been observed that the stiffness of the joint and bearing strength increase with the increase of the tightening torque.

As a result of the literature review, it was seen that many parameters affect the combination. Of these, it has been observed that the pre-tension load applied to the slip-critical joint significantly affects the capacity of the joint. At the same time, it is clear that friction on the joint contact surfaces is another parameter that affects the behavior of the joint. In this study, the effect of the joint on the bearing capacity was investigated by changing the pre-tensioning force, and the coefficient of friction between the plates (μ) parameters of the single-lap bolted joint.

2. Theoretical Background

This study aims to investigate the parameters that influence the load-carrying capability of friction-effect, single-lap, and single-bolt joints. In this setting, the analytical model of the joint requires stress analysis based on the theory of elastic mechanics. Since the stress distribution surrounding the bolt hole has a direct impact on the load-bearing capability of the joint, it is essential to investigate the load transfers, contact surfaces, and stress distributions in the joint in great detail.

In friction-effect, single-overlap, single-bolt connections utilizing high-strength bolts, the torque tension supplied to the bolt ensures that the joining plates are squeezed, thereby preventing the joint from dissolving under recurrent dynamic stresses. In this investigation, the condition in which the tightening torque of the single-lap joint, which is fastened from the left end of the upper plate and subjected to tensile stress from the right end of the lower plate, is applied has been considered. Fig. 1 depicts the problem's schematic depiction, the fastening tools (a high-strength bolt, a nut, and two washers), and the free body diagram of the joint under the influence of external loads.

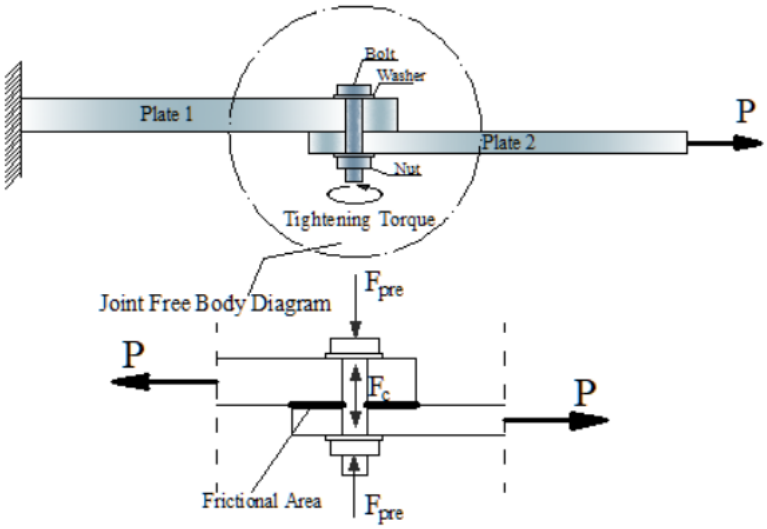

Fig. 1. Single lap bolted joint schema and joint free body diagram.

Examining the internal forces that develop in the plates and bolts under the acting loads independently is important for a thorough examination of the joint's load transfer. The washer behind the bolt head transferred the pre-tension load acting on the bolt (F_{pre}) to Plate-1 along the contact surface. Therefore, the response force (F_c clamped load) was created on the plates as a result of the pre-tensioning load squeezing the plates. Due to the action-reaction principle, the force F_c, which is equal and opposite to the front pulling force, is transferred to the head of the bolt by acting along the contact area between Plate 1 and the bottom of the washer. Plate 2 and the washer contact surface beneath the nut's bottom face experience a similar transfer of load.

In a friction-effective joint, the tensile stress applied in the direction of the plate axis causes the friction force (F_f) to act on the contact area of the plates in the overlapping regions. The frictional force is equal to the product of the normal force (N) perpendicular to the friction surface and the static friction coefficient (μ) of the friction surface (Fig.2).

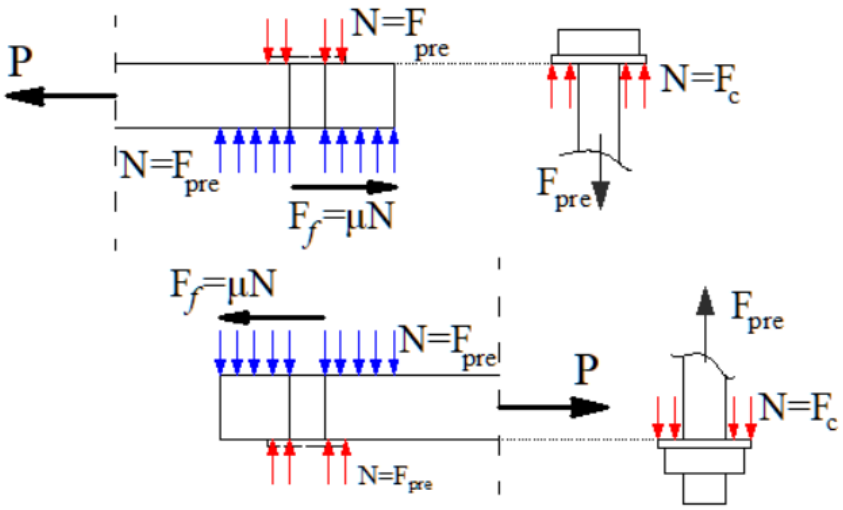

Fig. 2. Pre-tensioned bolted joint load transfer mechanism [12]

In the joint whose force distribution is shown in Fig. 2, the pre-tension load causes compressive stresses [$\sigma_n(x,y,z)$] on the contact surface beneath the bolt head, and the external force causes shear stresses [$\tau_n(x,y,z)$] in the contact region between the overlapping faces of the two plates. For elastic analysis of the joint with known contact areas and stress components, the stress distribution around the bolt hole can be determined analytically using equilibrium equations and elasticity relations [13]. When the derived equations are investigated, it becomes clear that a variety of variables affect the stress that forms around the bolted joint's hole. Analytical solutions are very expensive and difficult to use for examining parameter effects. To explore the impacts of parameters on both stresses and deformations, the finite element approach was chosen for this study. A solution is made by developing the spring model, which is also employed in the finite element method, for the analysis of the deformations of the bolted joint, for which the theoretical solution is known about stress analysis.

2.1. Load condition and spring model of single lap bolted joint

Figure 1 demonstrates that when a single external force is applied to the plate in a single-lap, single-bolt joint, the bolt is subject to bearing force (at bolt shank), shear force, and bending moment due to eccentric loading [14]. The loading conditions of the bolt are presented in Fig.3.

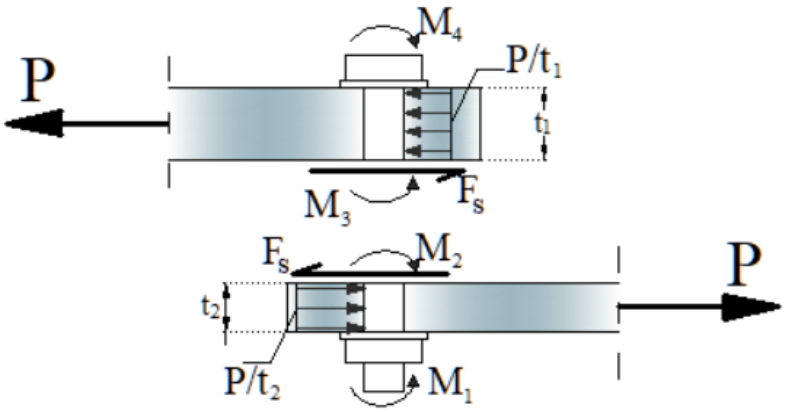

Fig. 3. Loading condition of bolt [14]

To calculate the stiffness and, thus deformations of the bolt in the studied joint, the bolt is modeled as a beam fixed at one end and with roller support at the other end under the load conditions shown in Fig. 3. The resulting statically indeterminate problem is solved by the superposition method and the deformations and stiffness of the bolt are obtained [14].

In this study, a spring model was first created considering the loading conditions in Fig. 3 (in the absence of pre-tensioning force) to find the displacements of the examined single-lap single-bolted joint (Fig. 4). Node displacements were calculated analytically by performing a static analysis of the spring model.

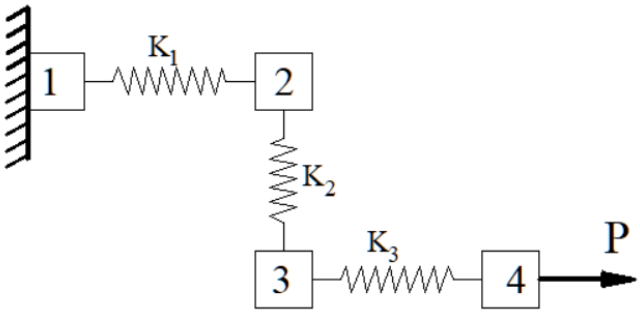

Fig. 4. Single-lap single bolted joint spring model

In the spring model presented in Fig. 4, the stiffnesses (K_1, K_3) of Plate 1 and Plate 2 are calculated by taking the equivalent stiffness AE/l. In contrast, the stiffness of the bolt (K_2), the $1/k_{eq}$ equation presented by Liu et al [14], was calculated by arranging it according to the material properties in this study (Eq. 1).

$$\frac{1}{k_{eq}}=\frac{4\left(t_1+t_2\right)}{9G_bA_b}+\frac{9\left(t_1^4+57t_1^3t_2+96t_1^2t_2^2+57t_1t_2^3+9t_2^4\right)}{384E_bI_b\left(t_1+t_2\right)}+\frac{1}{t_1E_b}+\frac{1}{t_2E_b}+\frac{1}{t_1E_{p1}}+\frac{1}{t_2E_{p2}} \tag{1}$$

Where G_b and E_b are the shear modulus and modulus of elasticity of the bolt, respectively. A_b and I_b are the cross-sectional area and moment of inertia of the bolt shank. E_{p1} and E_{p2} are the moduli of elasticity of Plate 1 and Plate 2, respectively. The equivalent stiffness (k_{eq}) of the bolt was calculated from the expression given in Eq. 1. Accordingly, the global stiffness matrix, global displacement, and force vectors of the spring model presented in Fig. 4 were written in the linear spring equation, then Eq. 2 was obtained by providing the boundary conditions of the problem (u_1=0).

$$\begin{bmatrix} K_1+K_2 & -K_2 & 0 \\ -K_2 & K_2+K_3 & -K_3 \\ 0 & -K_3 & K_3 \end{bmatrix}\begin{Bmatrix} u_2 \\ u_3 \\ u_4 \end{Bmatrix}=\begin{Bmatrix} 0 \\ 0 \\ P \end{Bmatrix} \tag{2}$$

The node displacements, u_2, u_3 and u_4, are determined by solving Eq.(2). Thus, the total displacement (u_4) of the single-lap bolted joint due to the axial tensile force applied to Plate 2 was determined. Using a similar method, the analytical solution of the pre-tensioned joint, which is the central issue of this paper, is derived by adjusting the load vector accordingly. In the third section, numerical results gained are presented.

3. Numerical Analysis

During the numerical analysis of the single-lap, single-bolted joint, the model geometry and bolt placement should be determined. For this, the model in [15], which is a similar study in the literature, was taken as a reference regarding its geometric properties and bolt assembly selection.

The finite element model of the single-overlap and single-bolt friction-effect joint was created with the 'Space Claim Cad software. By predicting the boundary conditions to be applied in the finite element solution of the problem (as 220mm of the plates is represented as the attachment

surface), a 3D solid model of the joint was constructed. Detailed diagrams of the joint are provided in Fig. 5.

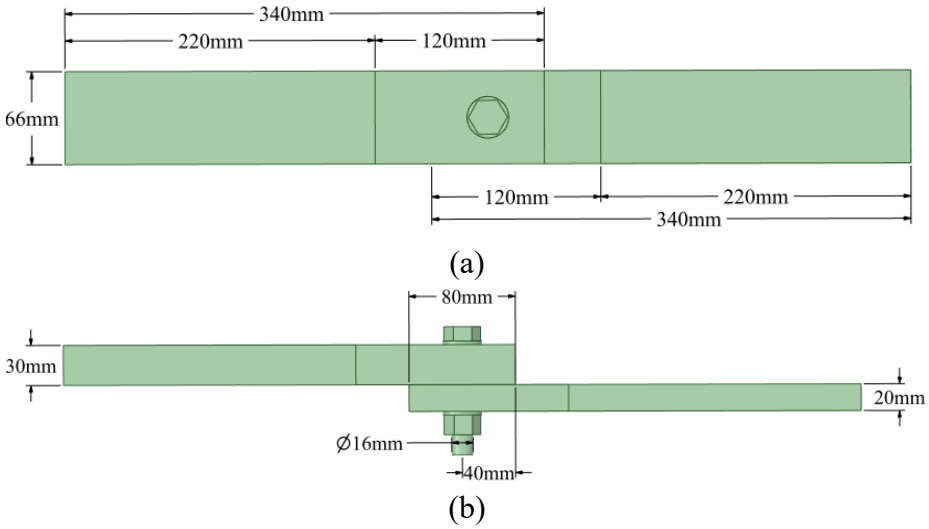

Fig. 5. Single-lap joint geometric detail (a)top view (b) front view

The Specification for the Design, Calculation, and Construction of Steel Structures mandates the use of high-strength (8.8 or 10.9) bolts in pre-tensioned joints with friction effect. In this study, class 8.8 M16 bolts and appropriate washer-nut jointing equipment were utilized. Both joining plates are made of S235-grade structural steel. Table 1 lists the material type, yield strength, tensile strength, and relevant standards for the bolt and plate selected for numerical analysis. In the connection's numerical analysis, the general-purpose ANSYS [16] application employing the finite element method was utilized. The Space Claim-created solid model of the problem was transferred to the ANSYS Workbench simulation environment for finite element solutions.

Table 1. Characteristic strength of materials (MPa)

Material Class	F_y *(N/mm²)*	F_u *(N/mm²)*	*Standard*
Plate/S235	235	360	EN 10025-2
Bolt/8.8	640	800	EN 14399

3.1. Defining material models

After creating a 3D geometric model of the problem, acceptable material models for the plate and bolt elements were chosen to depict the specified materials' behavior accurately, and their mechanical properties were described. For the plates and joint tools, the 'Structural Steel NL' material model from the material library that permits plastic analysis was chosen (bolt, nut, and washer). The 'Bilinear Isotropic Hardening' plasticity model represents, by default, the plastic behavior of structural steel in the given material model. Table 2 presents the material attributes defined for the program.

Table 2. Mechanical properties of materials

Mechanical Properties and Units	***Plate1 and Plate 2 S235***	***Bolt, Nut and Washer 8.8***
Modulus of Elasticity € (Gpa)	200	200
Shear Modulus (G) (*Gpa*)	76.92	76.92
Poisson Ratio (ν)	0.3	0.3
Yield Strength (σ_y) (Mpa)	235	640
Ultimate Strength (σ_u) (Mpa)	360	800

3.2. Finite element modelling

After defining the material parameters of the fastening tools (a bolt, nut, and two washers) and connecting components (two steel plates) that comprise the single-lap bolted joint, the ANSYS Workbench Mechanical component was utilized to generate the finite element model and was performed the analysis. The mechanical component is a simulation module with 3D analytical tools. Elements of plates, bolts, nuts, and washers were modeled using a SOLID186 element model with 20 nodes [16].

Determining the contact properties between the contact surfaces of the elements in modeling the problem is important in terms of the analysis results and the realistic representation of the joint behavior. The ANSYS program automatically creates the contact elements after the problem geometry is loaded into the Mechanical component. However, the selection made by the program is not always the desired accuracy and feature. For this reason, the contact definition of the junction model was made manually, considering the contact surface properties, element behavior, and load transfer. Contact identification in ANSYS is made with the 'contact-target' approach [16]. Eight different 'contact surfaces' are defined in this model. These; washer bottom surface-Plate1 upper surface, two washers inner surface-bolt shank, nut inner surface-bolt thread part, bolt shank-hole, Plate1 bottom surface-Plate2 upper surface, washer upper surface-bolt head bottom surface, washer bottom surface- nut upper surface and washer upper surface-Plate 2 is bottom surface.

After the contacts were defined, the mesh procedure, which significantly impacted the analysis stages and the verification of the results to be obtained, was started. In the investigated problem, since the periphery of the hole and the contact surface of the thin washer element are critical areas where stress concentrations occur, meshing should be done in more detail, especially in such areas. The meshing method and the choice of element size to be used affect the analysis results as well as the analysis time. Therefore, it is important to make the optimum choice. In the study, the mesh sensitivity was increased in these regions by reducing the element size in the area of the joint and the elements that provide load transfer with the contact surface. The meshing process was performed by selecting the appropriate method and size for each plate, bolt, nut, and washer element.

The boundary conditions of the problem are fixed at the left end of Plate 1 and applied as u_y =0 and u_z =0 on 220mm long parts of the plates to prevent secondary bending effects. An axial tensile force F=10 kN was applied from the free end of Plate 2. The generated numerical model is presented in Fig.6.

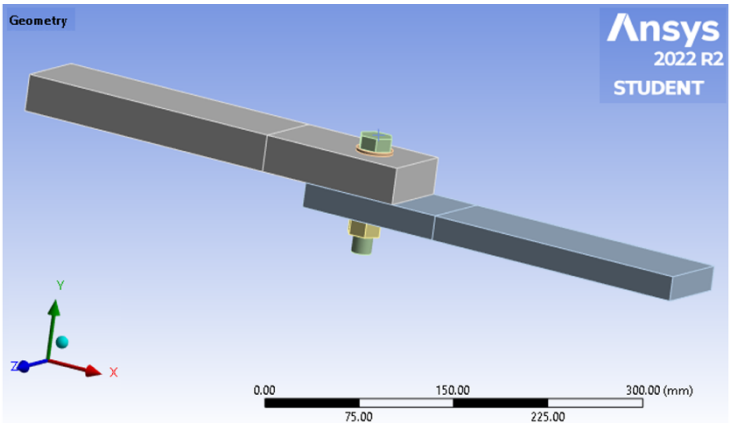

Fig. 6. Finite element model of single lap bolted joint

The static analysis of the single-lap bolted joint, completed for the finite element solution, has been done, and the results of Equivalent Stress and total deformation are presented in Fig. 7.

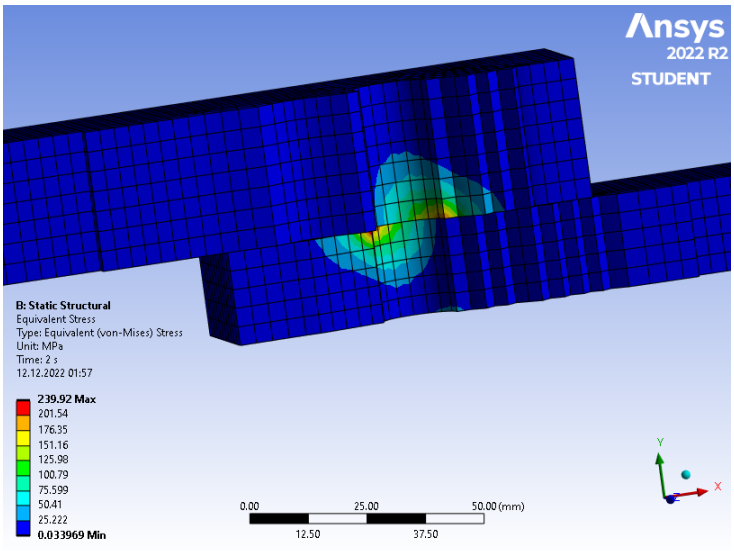

(a)

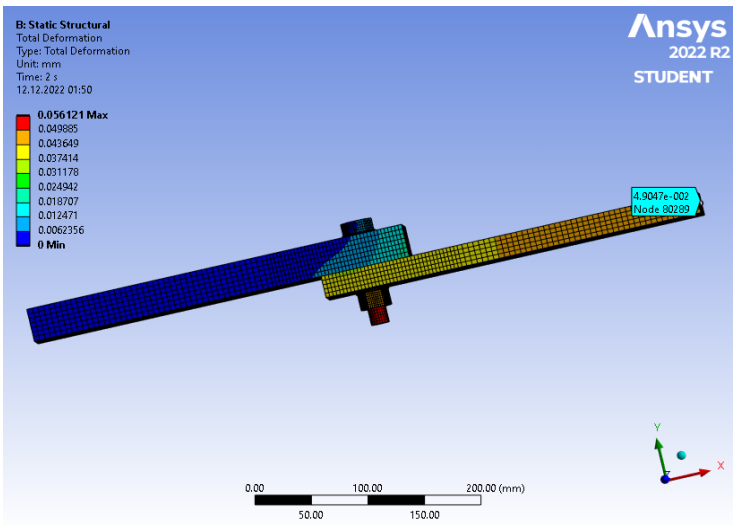

(b)

Fig. 7. FE analysis results (a)equivalent stress of plates (b)total deformation of model

When Fig. 7(a) is examined, it is seen that the stress distribution reaches the maximum values around the hole as predicted. It is seen that the Equivalent Stress plates reach the yield value while local crushing occurs around the hole under the effect of a 10 kN external load applied.

Model validation was performed by comparing the displacement of node 4 (u_4) obtained from the solution using the spring model in Section 2.1 with the displacement of the free end of Plate2 presented in Fig. 7(b). The results obtained are given in Table 3.

Table 3. Spring and Numerical model deformation results

	U_4 (mm)
Spring Model	0.05312
Numerical Model	0.04907

It is seen that there is a difference of 4μm between the results obtained from the two different models. It is thought that this difference is due to the assumptions made to simulate the real problem and the solution methods used.

4. Results and Discussions

The theoretical analysis of friction-effect joints was made in Section 2. As a result of this examination showed that the contacting surface areas, pretension load, friction coefficient, etc. parameters were influential in the stress distribution and deformations around the hole. In this part of the study, the effects of pretension load and friction coefficient parameters on the bearing capacity of the joint were investigated using the validated finite element model. Obtained results are presented in separate sections for each parameter.

4.1. Effect of prentension load

In the study, three different pretension load values, 10kN, 15kN, and 20kN, were taken, and stress and deformation analyses of the single-lap bolted joint was performed. The σ_{eq} and total deformation results obtained for F_{pre}=20kN are presented visually in Fig. 8, and other values are given in Table 4.

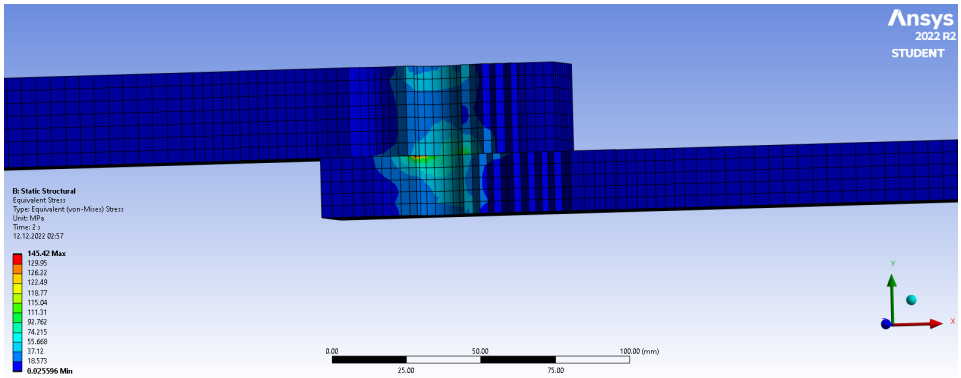

(a)

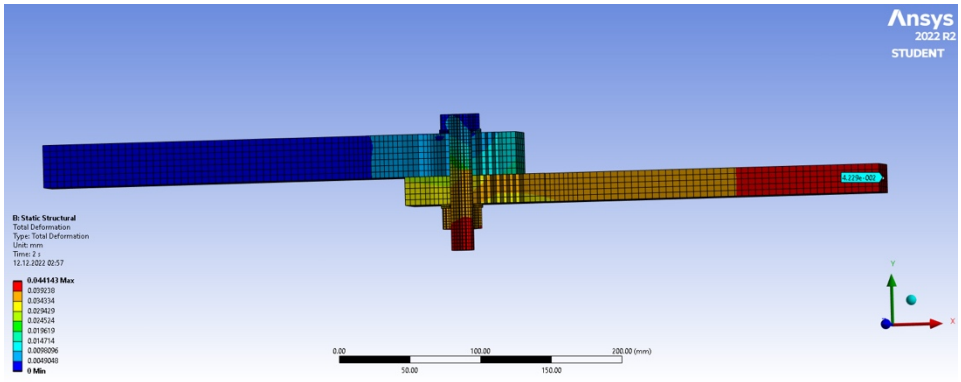

(b)

Fig. 8. FEA results when F_{pre}=20kN (a)equivalent stress of plates (b)total deformation of the model

According to the results given in Fig. 8(a) and 8(b), the greatest equivalent stress in the plates is σ_{eq}=145.52MPa, and the displacement of the free end is u_4=0.04229mm. If these results are compared with the 'Basic Model,' it is seen that the stress distribution around the hole and the displacement of the free end decrease when the pretension load is applied. Considering these results, it can be said that all models with pre-tensioning loads show linear behavior, so they do not reach yield load. Since the yield strength is reached under the effect of a load of F=10kN applied to the basic model, the yield load ($F_{y\text{-numerical}}$) of the models with pre-tension are calculated with the inverse ratio between the stresses and the applied force.

Table 4. Pretension Load effect of numerical yield load

Pretension Load (kN)	*Friction Coefficient*	σ_{eq} (MPa)	$F_{y\text{-numerical}}=F(\sigma_y/\sigma_{eq})$
0	0.2	239.92	9.8kN
10	0.2	184.13	12.76kN
15	0.2	164.69	14.27kN
20	0.2	145.52	16.15kN

According to the results presented in Table 4, it is seen that increasing the pre-tensioning force increases the load-carrying capacity of the joint. It was concluded that the capacity of the joint increased by 30.2% when the pretension load was 10kN, by 45.61% when it was 15kN, and by 64.8% when the pretension was not applied.

In Fig. 9, graphs of the Net Force (F_{Net}) and displacement (u_4) of Plate 2, depending on the pre-tension load change, are given. The net force is the difference of F=10kN applied to the free end of Plate 2 and the *x* component of the frictional force on the contact surface between the plates. According to the results, as the preload increased, the friction force increased, so the F_{Net} decreased, and accordingly, the displacement decreased.

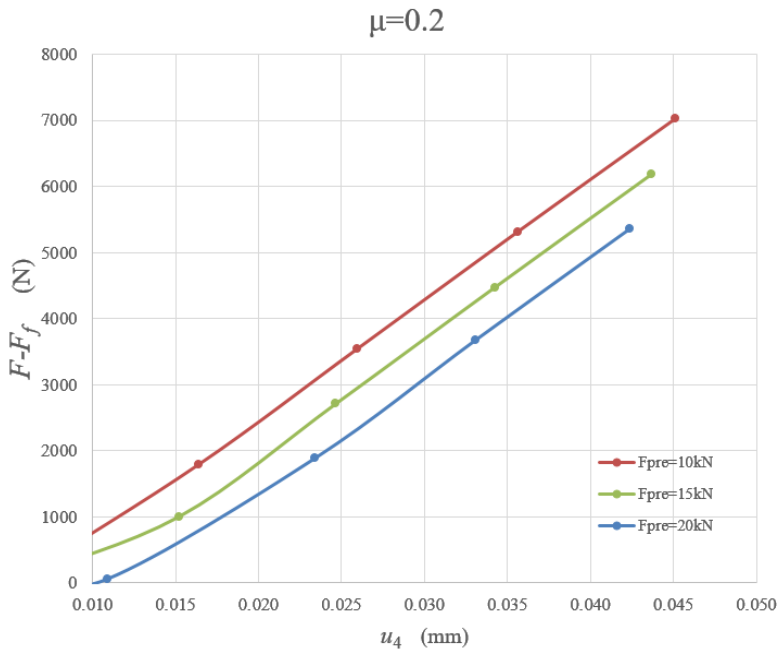

Fig. 9. Effect of pretension load to total deformation

4.2. Effect of friction coefficient

The values to be used in examining the effect of the friction coefficient parameter are taken from the TSEN 1090-2 Standard. By choosing three different friction coefficients μ=0.1, 0.2, 0.3, analyzes were made in the loading condition where F=10kN and F_{pre}=15kN. Equivalent stress and total deformation results obtained for the case where μ=0.3 are presented visually, and other values are given in Table 5 and Fig.10.

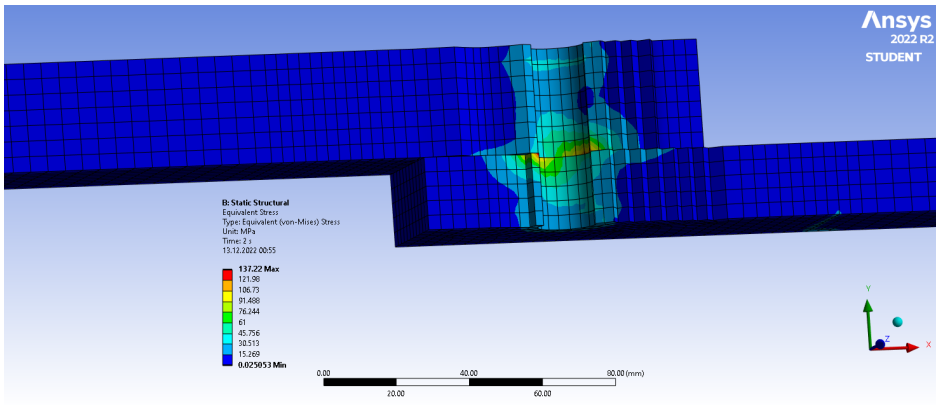

(a)

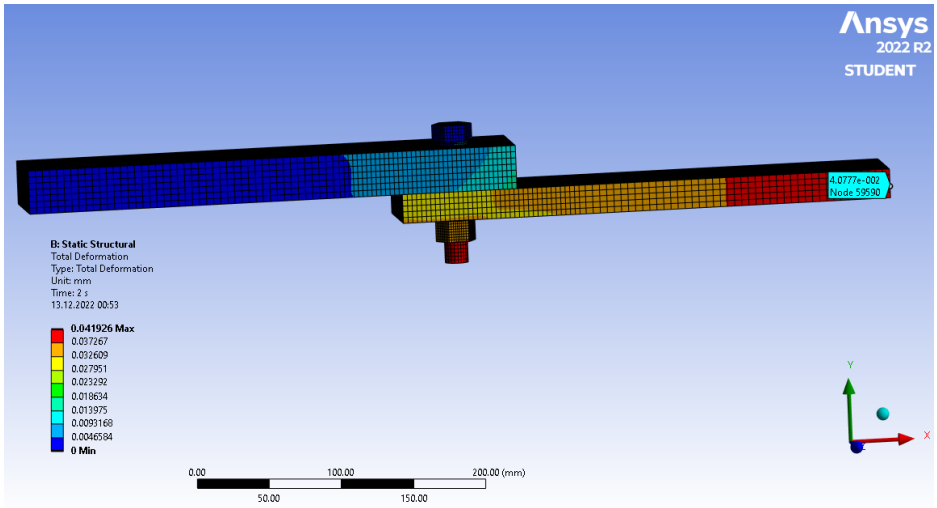

(b)

Fig. 10. FEA results when μ=0.3 (a)equivalent stress of plates (b)total deformation of model

Table 5. Friction Coefficient effect of numerical yield load

Friction Coefficient	*Pretension Load (kN)*	σ_{eq} (MPa)	$F_{y\text{-}numerical}=F(\sigma_y/\sigma_{eq})$
0.1	15	194.25	12.10kN
0.2	15	164.69	14.27kN
0.3	15	137.22	17.13kN

When Fig. 10(a) and (b) are examined, it is seen that the stress and total deformation decrease with the increase in the friction coefficient. Therefore, the F_{net} force applied to Plate 2 decreased in this case. According to the results in Table 5, the bearing capacity decreased by 15% when the friction coefficient was 0.1 and increased by 20% when the friction coefficient was 0.3, compared to the situation with a friction coefficient of 0.2 and F_{pre}=15kN. The results show that the friction coefficient is another parameter that increases the joint capacity.

5. Conclusions

This study investigated the parameters affecting the bearing capacity of the single-lap frictional joint. First, a solution method for calculating the node displacements was developed by creating the spring model of the problem. Then, a numerical model was created, and this model's nonlinear analysis was made under the axial tensile load's effect, and the yield load was determined. In addition, the displacements obtained from this analysis were compared with the results obtained from the spring model, and numerical model validation was performed.

During the parametric study, the pretension load and friction coefficient values were determined, verified, and applied to the Basic Model. The joint's capacity load was calculated using a similar calculation method for both parameters.

It has been noticed that the equivalent stresses around the hole diminish as the pretension load increases from 10kN to 15kN to 20kN; thus, the predicted capacity load increases. Simultaneously, when the pretension load increased, the friction force acting on the contact surface of the plates increased, and the influence of the external force reduced. Therefore, this circumstance likewise lowered the displacements of Plate 2's free end, where the F_{Net} force acts.

Since the effect of the friction coefficient parameter is directly proportional to the friction force, it was quite similar to the pretension load. With the increase of the friction coefficient, both the stresses around the hole and the displacements of the free end of the plate decreased. This result shows that the surface roughening processes on the plates are also suitable for increasing the capacity of the joint. Thus, it is seen that the capacity can be increased by roughening as an alternative to the application of increasing the pretension load.

References

[1] Ministry of Environment and Urbanisation, Specification for Design and Construction of Steel Structures, Republic of Turkey Ministry of Environment and Urbanisation, Ankara,Turkey, 2016.

[2] Sudev, L.J. and Gajendra, S., Strength analysis of single lap dissimilar materials bolted joint. *In IOP Conference Series: Materials Science and Engineering*, 390(1), 2018.

[3] Riccio, A., Effects of geometrical and material features on damage onset and propagation in single-lap bolted composite joints under tensile load: part ii–numerical studies. *Journal of Composite Materials*, 39(23), 2091-2112, 2005.

[4] Da Silva, L.F., Rodrigues, T.N.S.S., Figueiredo, M.A.V., De Moura, M.F.S.F., Chousal, J.A.G., Effect of adhesive type and thickness on the lap shear strength. *The Journal of Adhesion*, 82(11), 1091-1115, 2006.

[5] Ireman, T., Three-dimensional stress analysis of bolted single-lap composite joints. *Composite Structures*, 43(3), 195-216, 1998.

[6] Sinthusiri, C. and Nassar, S.A., Load Distributions in Bolted Single Lap Joints Under Non-Central Tensile Shear Loading. *Journal of Advanced Joining Processes*, 3, 2021.

[7] McCarthy, C.T. and McCarthy, M.A., Three-dimensional finite element analysis of single-bolt, single-lap composite bolted joints: Part II—effects of bolt-hole clearance. *Composite Structures*, 71(2), 159-175, 2005.

[8] Saraç, İ., The numerical investigation of the effects of hole tolerance and bolt torque variation on the joint strength in the bolted joints. *Journal of the Faculty of Engineering and Architecture of Gazi University*, 37(2), 685-695, 2022.

[9] Ghanbari, E., Sayman, O., Ozen, M., Arman, Y., Failure load of composite single-lap bolting joint under traction force and bending moment. *Australian Journal of Basic and Applied Sciences*, 6(9), 683-692, 2012.

[10] Chakherlou, T.N. and Jirandehi, A.P., A profound study on the effects of friction coefficient on torque tightened, longitudinally loaded, bolted connections. *The 1st conference on Modern Achievements in Aerospace and Related Sciences*, Tehran, Iran, 2015.

[11] Khashaba, U.A., Sallam, H.E.M., Al-Shorbagy, A.E., Seif, M.A., Effect of washer size and tightening torque on the performance of bolted joints in composite structures. *Composite Structures*, 73(3), 310-317, 2006.

[12] Varma, A, Design of Steel Structures Lecture Notes. https://www.egr.msu.edu/~harichan/classes/ce405/chap5.pdf, 2002.

[13] Liu, W. and Lin, W., Stress around the hole of single lapped and single bolted joint plates with fitting clearance. *Journal of Mechanical Science and Technology*, 33(4), 1623-1632, 2019.

[14] Liu, L., Mao, Y., Wei, R., An analytical tool to predict load distribution of multi-bolt single-lap thick laminate joints. *In Proceedings of the 18th International Conference on Composite Materials*, Korea, 2011.

[15] Pawar, J.S., Chouksey, M., Tripathi, K., Modeling and stress analysis of single lap bolted joint. *Universal Journal of Mechanical Engineering*, 3(1), 21-26, 2015.

[16] Kohnke, P., *Theory reference for the mechanical APDL and mechanical applications*, Ansys, Inc, Canonsburg, 2009.

International Journal of Engineering & Applied Sciences (IJEAS)
Vol.14, Issue 3 (2022) 91-99
http://dx.doi.org/10.24107/ijeas.1223750
Int J Eng Appl Sci 14(3) (2022) 91-99

Probabilistic Seismic Hazard Analysis of Burdur City

Mehmet Alpyürür

Burdur Mehmet Akif Ersoy University, Civil Engineering Department, Burdur-TURKIYE
**E-mail address:* malpyurur@mehmetakif.edu.tr

ORCID numbers of author:
0000-0002-6878-5874

Received date: 24.12.2022
Accepted date: 31.12.2022

Abstract

This study's objective is to evaluate the seismic risk for Burdur City (SW Turkey) using a probabilistic methodology. Within the framework of the study, a new earthquake catalog for Burdur City and the surrounding area was created with a unified moment magnitude scale. The region's seismicity was assessed using the Gutenberg-Richter recurrence relationship. Software called R-CRISIS (v18) was used to calculate risks. Analyses were conducted using New Generation Attenuation models. With hazard levels of 2% and 10% probability of exceedance in 50 years, seismic hazard maps for the peak ground acceleration and bedrock were created. The study's findings indicate that peak ground acceleration values on bedrock vary between 0.70-0.75 g and 0.44-0.48 g, respectively, for hazards levels of 2% and 10% probability of exceedance in 50 years.

Keywords: Burdur, Seismic hazard analysis, PGA, R-CRISIS

1. Introduction

The danger posed to civilization by devastating earthquakes in many regions of the globe is sufficient justification for evaluating the seismic hazards of earthquakes while constructing buildings and infrastructures [1,2,3]. As a result of the region's high seismic activity, a number of researchers have evaluated the seismic hazard of several areas in southwest Turkey [4,5,6,7,8].

The Burdur Basin and its environs are situated in a region that has seen high seismic activity over both the historical and instrumental periods [9]. On October 3, 1914, and May 12, 1971, there were two large earthquakes. Both events created extensive damage. The earthquake that occurred on October 3, 1914 (Ms:7.0) was the largest of the two, killing about 4000 people and demolishing 90 percent of Burdur's residences. The May 12, 1971, incident (Ms:6.2) produced more localized devastation and resulted in the deaths of 57 persons. These events caused surface fault ruptures [10].

Western Turkey, situated at the eastern extremity of the Aegean Extensional Province, represents one of the biggest instances of active continental expansion [11]. Numerous academics have examined the Western Anatolia tectonic area to determine the relationship between relative plate motions and complicated tectonic features. The horst-graben system in this region, which comprises the Edremit, Bakırçay, Kütahya, Simav, Gediz, Küçük Menderes, Büyük Menderes, and Gokova grabens, is considered to be one of the most active extensional tectonic structures in the world, with an average GPS velocity of 20 mm/yr [12].

Burdur city center is located on the Burdur fault, one of the most important active faults in Western Anatolia, located in the Fethiye-Burdur fault zone. An important part of Burdur city

center is located on Quaternary lacustrine sediments and young creek alluvium. When the tectonic environment of the city is considered together with its geotechnically unfavorable situation, the seismic vulnerability increases. In the present research, seismic hazard study was conducted for Burdur City using a probabilistic approach. Western Anatolia (WA), between 34° and 40° N latitudes and 26° and 33° E longitudes, was considered as seismic study region for the evaluation of seismic hazards.

2. Method

2.1 Seismicity model

The Modified Gutenberg-Richter seismicity model [13], that is related to Poissonian occurrences, was applied in the Probabilistic Seismic Hazard Analysis (PSHA) computations using the R-CRISIS v18 [14] program. The phase of intensity exceedance maintains the Poissonian procedure, together with the Poissonian occurrences. According to the Poissonian procedure, the possibility that an intensity would above a certain level during the next t years becomes as follows:

$$\Pr\,(A > a|t) = 1 - \exp[-\upsilon(a)t] \tag{1}$$

where $\upsilon(a)$ is the exceedance frequency of intensity a. If an event of magnitude M occurs at a hypocenter distance r from the chosen site, the Modified Gutenberg-Richter seismicity model predicts that the chance of hazard intensity above a threshold in the next t years will be estimated by the following formula:

$$P_E(a,t|M,r) = 1 - \exp[-\Delta\lambda(M)t.p_1(a|M,r)] \tag{2}$$

where, $p_1(a|M,r)$ is the exceedance probability of the hazard intensity a, assuming that an earthquake of magnitude M occurred at a hypocenter distance r from the point of interest. The Poissonian magnitude exceedance frequency, $\Delta\lambda(M)$, is determined by the magnitude range that magnitude M defines as in Eq. 3:

$$\Delta\lambda(M) = \lambda\left(\frac{M-\Delta M}{2}\right) - \lambda\left(\frac{M+\Delta M}{2}\right) \tag{3}$$

The modified Gutenberg-Richter model [15] gives the Eq. 4 for the exceedance frequency of the earthquake magnitude M:

$$\lambda(M) = \lambda_0 \frac{\exp(-\beta M) - \exp\,(-\beta M_{max})}{\exp(-\beta M_{min}) - \exp\,(-\beta M_{max})}, M_{min} \le M \le M_{max} \tag{4}$$

where M_{min} is the threshold earthquake magnitude and λ_0 is the exceedance frequency of the M_{min}. β represents a seismicity parameter equal to the natural logarithm of "b" value, and M_{max} denotes the predicted maximum earthquake magnitude for the seismic source.

2.2 Earthquake data and seismic source zones

The first step in this PSHA is creating an earthquake catalog for the region, that is homogenized and declustered, and identifying of the seismic sources that may produce ground motions at the region. The seismicity of WA was studied by different researchers. They suggested different zonation models related to WA. In this study, the zonation model containing 15 seismic regions

suggested by Bayrak and Bayrak [16] is used. Earthquake epicenter distribution and seismic sources are shown in Figure 1.

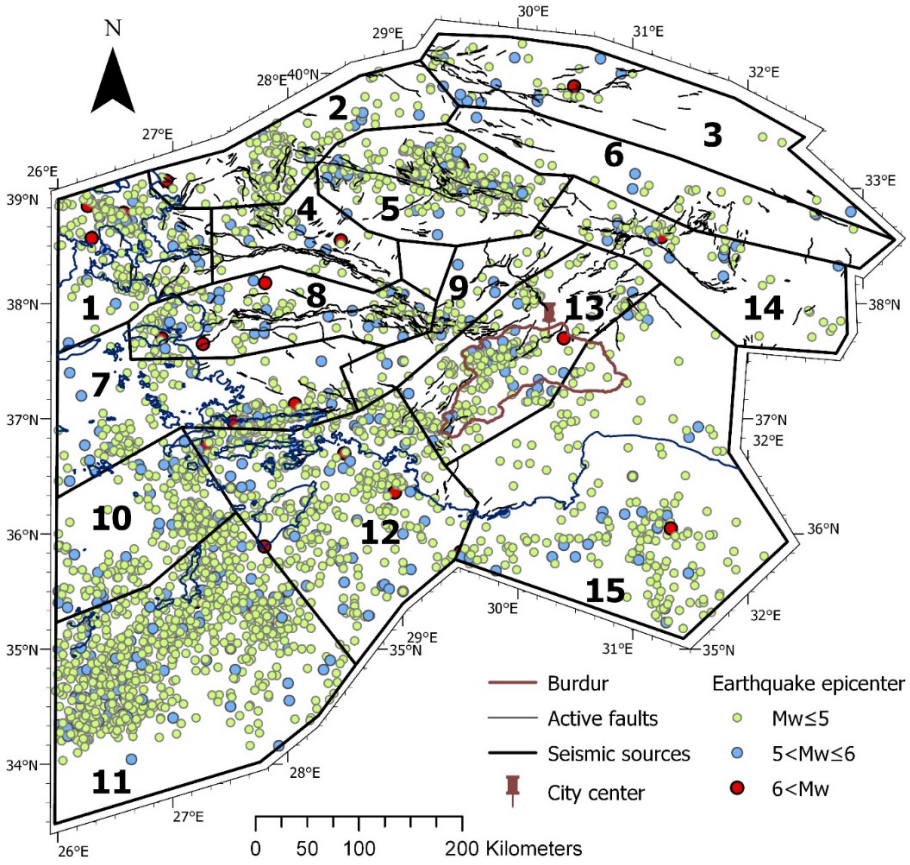

Fig.1. Location of earthquake epicenters and 15 main seismic sources in SW Turkey.

In this study only instrumental shallow earthquake (h < 70 km) data was used. The earthquake data from 1900 to 2005 was obtained from Kalafat et al. [17] and the data from 2005 to 2020 was obtained from the earthquake catalog of the Disaster and Emergency Management Presidency of Turkey. Data homogeneity is essential to the analysis. For this reason, the following magnitude conversion equations provided by Akkar et al. [18] were utilized to convert different magnitude scales, including body wave magnitude (Mb), surface wave magnitude (Ms), local magnitude (Ml), and duration magnitude (Md), to moment magnitude (Mw) in order to achieve magnitude scale homogeneity.

$$Mw = 0.5716(\pm 0.024927)Ms + 2.4980(\pm 0.117197),\ 3.4 \leq Ms \leq 5.4 \quad (5)$$

$$Mw = 0.8126(\pm 0.034602)Ms + 1.1723(\pm 0.208173),\ 5.5 \leq Ms \quad (6)$$

$$Mw = 1.0319(\pm 0.025)Mb + 0.0223(\pm 0.130) \quad (7)$$

$$Mw = 0.7947(\pm 0.033)Md + 1.3420(\pm 0.163) \quad (8)$$

$$Mw = 0.8095(\pm 0.031)Ml + 1.3003(\pm 0.154) \quad (9)$$

The completeness of the earthquake data is another important criterion for the analysis. In other words, the catalog must contain all of the events with magnitudes greater a specific minimum (cut-off) magnitude (Mc) that occurred in a particular seismic source over a particular time

period. The selection of the main shocks from the earthquake catalog is another basic consideration. For usage in the Gutenberg-Richter equation, the catalog must be free of all after- and for-shocks. For this reason, these dependent events, after- and for-shocks, were exluded from the catalog using Reasenberg's [19] declustering approach. In this study, Mc, a and b parameters were determined using the ZMAP (v7) software developed by Wiemer [20], where the maximum likelihood method suggested by Aki [21] is applied. The Gutenberg-Richter recurrence relationship was utilized to assess the seismicity of the seismic sources. This well-known equation has the following general form:

$$LogN(M) = a - bM \tag{10}$$

where N(M) (cumulative frequency), is the number of earthquakes equal or larger than M magnitude. The magnitude-frequency relation's variables (a) and (b) denote constants. The average yearly seismic activity index is defined by value (a), which is dependent on the observation period and the seismic activity. The slope of the linear function is provided by parameter (b), which relates to the physics of earthquakes.

It is essential to understand how ground motions attenuate with distance in order to assess the seismic risk at a given location. This statement, often known as the law of attenuation, connects magnitude, distance, and seismic intensity. The impact of the earthquake's size will be lessened by the larger the distance between the rupture area and the location where the risk is assessed [22]. Usually, empirical attenuation relationships, in other words Ground Motion Prediction Equations (GMPE), constrain how PGA values reduce with distance. The Turkish earthquake database is largely dominated by 1999 Kocaeli and Düzce earthquakes with lower intensities; there are no seismological indications that this pattern will be endorsed by potential large magnitude occurrences [23]. Hence GMPEs derived from global database were preferred in this study. Attenuation models developed by Abrahamson et al. - ASK14 [24], Campbell and Bozorgnia - CB14 [25], Chiou and Youngs - CY14 [26], Boore et al. - BSSA14 [27], Idriss - I14 [28], Akkar et al. - ASB14 [29] and Derras et al. - D16 [30] are examined with different earthquake scenarios, and ASK14, CB14, and CY14 models were selected according to the results shown in Figure 2.

For hazard computation, R-CRISIS v18 software was used. This program complies to the Cornell [31] approach. This technique integrates the effect of all probable seismic sources, assigns their average activity rate, and then analyzes the seismic hazard at the location of interest.

The creation of hybrid GMPE models with selected GMPEs and assigned branch weights constitutes the final stage of the analysis. After examining 7 GMPEs chosen for active shallow crustal earthquakes, 3 of them (ASK14, CB14, and CY14) were selected for hybrid model (HM) applications, and 6 different hybrid GMPE models were created as shown in Table 1.

Table 1. Hybrid models and weights of selected GMPEs.

	HM1	HM2	HM3	HM4	HM5	HM6
ASK14	0.4	0.3	0.3	0.5	0.25	0.25
CB14	0.3	0.4	0.3	0.25	0.5	0.25
CY14	0.3	0.3	0.4	0.25	0.25	0.5

Earthquake recurrence parameters were determined by carrying out calculations using a maximum-likelihood approach within the ZMAP (v7) software. Earthquake hazard parameters for 15 different seismic sources are given in Table 2.

The M_{max} value represents the highest predicted magnitude of an earthquake for each source zone. It is expected that no source will generate an earthquake with a magnitude larger than the predicted M_{max}. In the present study, M_{max} value was estimated by adding a constant value to

maximum observed magnitude (M_{max}^{obs}). Different maximum probable magnitudes of each source were predicted as M_{max}^{obs}, M_{max}^{obs}+0.3, and M_{max}^{obs}+ 0.5. Seismic hazard calculations for Burdur city were conducted for each hybrid GMPE models and M_{max} combinations.

Table 2. Calculated earthquake hazard parameters for 15 different seismic regions by ZMAP.

Source no	Tectonics	M_{max}^{obs}	a	b	Mc
1	Aliağa Fault	6.4	5.54	0.81	4.2
2	Akhisar Fault	6.0	5.99	0.91	4.2
3	Eskişehir, İnönü Dodurga Fault Zones	6.3	4.28	0.83	4.0
4	Gediz Graben	6.3	4.69	0.81	4.1
5	Simav, Gediz-Dumlupınar Faults	6.2	6.23	0.91	4.3
6	Kütahya Fault Zone	6.5	5.40	0.82	4.4
7	Karova-Milas, Muğla-Yatağan Faults	6.4	5.82	0.85	4.2
8	Büyük Menderes Graben	6.5	5.29	0.83	4.2
9	Dozkırı-Çardak, Sandıklı Faults	6.0	5.19	0.85	4.2
10	Aegean Islands	6.0	6.22	0.93	4.1
11	Aegean Arc	7.0	6.32	0.84	4.2
12	Aegean Arc, Marmaris, Köyceğiz, Fethiye Faults	6.5	5.89	0.81	4.2
13	Gölhisar-Çameli, Acıgöl, Tatarlı Kumdanlı Faults, Dinar Graben	6.6	5.98	0.87	4.0
14	Sultandağı Fault	6.5	5.27	0.80	4.1
15	Beyşehirgölü, Kaş Faults	6.1	5.87	0.88	4.1

3. Results

The findings of the seismic hazard assessments for the Burdur City center, including PGA (peak ground acceleration), T=0.2s and T=1s spectral acceleration values, are depicted in Table 3.

Table 3. Values of PGA and spectral accelerations for bedrock level, in units of g, for periods of 0.2 and 1s, with 10% and 2% probability of exceedance (PoE) in 50 years.

		$\mathbf{M_{max}^{obs}}$			$\mathbf{M_{max}^{obs}+0.3}$			$\mathbf{M_{max}^{obs}+0.5}$		
		PGA	0.2s	1s	PGA	0.2s	1s	PGA	0.2s	1s
10% PoE in 50 yr (475-yr return period)	HM1	0.409	0.985	0.270	0.479	1.200	0.350	0.537	1.380	0.411
	HM2	0.404	0.959	0.264	0.466	1.150	0.339	0.514	1.300	0.395
	HM3	0.396	0.950	0.260	0.458	1.140	0.335	0.510	1.300	0.391
	HM4	0.417	1.010	0.277	0.497	1.260	0.363	0.562	1.460	0.428
	HM5	0.405	0.950	0.262	0.459	1.130	0.335	0.504	1.260	0.388
	HM6	0.385	0.927	0.253	0.444	1.110	0.325	0.494	1.260	0.379
2% PoE in 50 yr (2475-yr return period)	HM1	0.649	1.610	0.430	0.748	1.920	0.601	0.820	2.130	0.697
	HM2	0.639	1.570	0.419	0.724	1.840	0.576	0.789	2.040	0.672
	HM3	0.630	1.560	0.413	0.719	1.840	0.568	0.786	2.040	0.667
	HM4	0.663	1.650	0.444	0.772	1.990	0.624	0.849	2.220	0.722
	HM5	0.638	1.550	0.415	0.714	1.810	0.566	0.773	1.990	0.661
	HM6	0.615	1.520	0.400	0.701	1.790	0.546	0.766	1.990	0.648

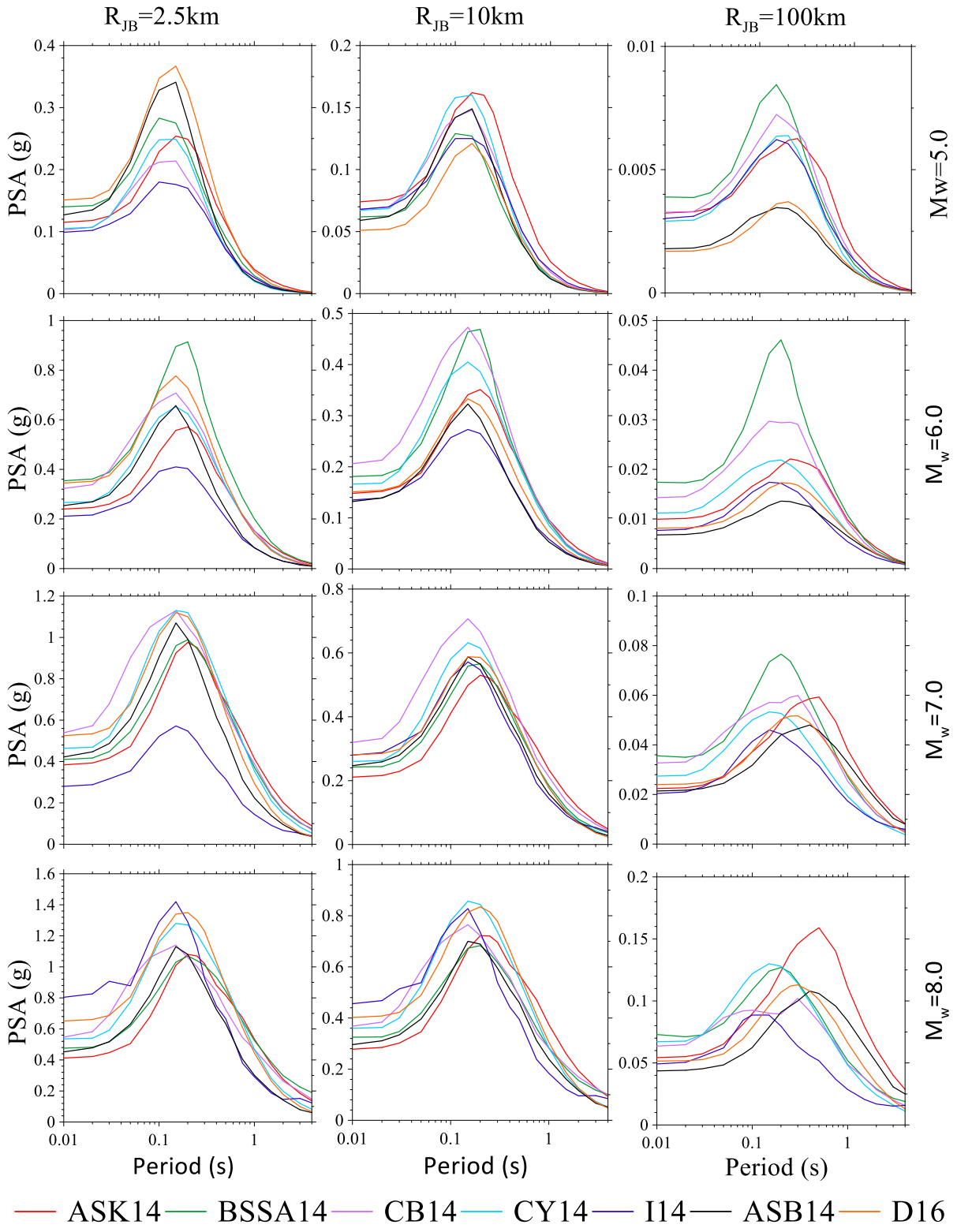

Fig. 2. Response spectrum of examined GMPEs (V_{s30}=760 m/s, H=10km, Z_{TOR}=0, Dip=90, Strike=180, K_1=0.0038, K_2=1.15).

Results of the probabilistic seismic hazard analyses show that in the city center of Burdur, PGA values for M_{max}^{obs} + 0.3 and for hazard levels of 2% and 10% probability of exceedance in 50

years change with HMs between 0.70-0.75 g and 0.44-0.48 g, respectively. Seismic hazard maps of Burdur City in terms of PGA values for HM3 and M_{max}^{obs}+0.3 are shown in Figure 3.

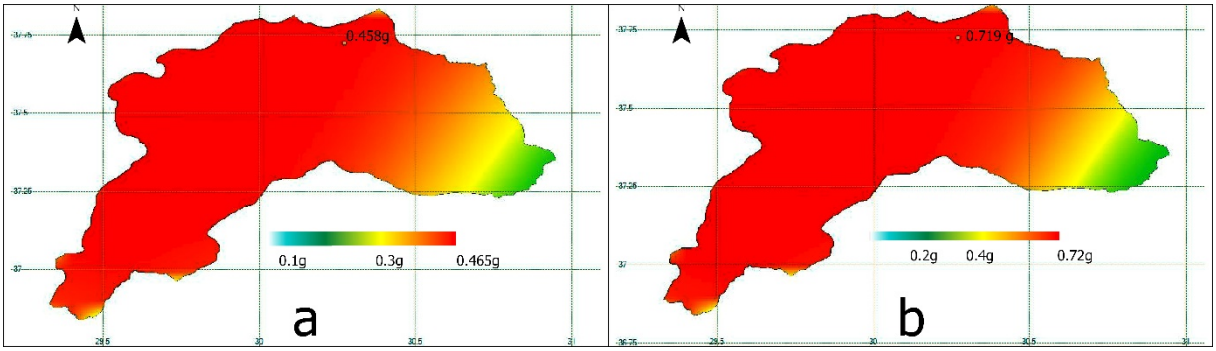

Fig. 3. PGA values of PSHA with HM3 and M_{max}^{obs}+0.3; a) 475 and b) 2475-year return periods

4. Conclusions

The city center of Burdur is mostly built on loosely constructed new alluviums and accumulation cones. The Burdur city center is largely established on the Fethiye-Burdur Fault Zone (FBFZ), one of the most important active faults in Western Anatolia. When these two situations are evaluated together, it is concluded that the seismic risk for the Burdur settlement area is high. Burdur and comparable areas are thus in serious need of any and all scientific research that can aid in the evaluation of seismic risks. In this study, the seismic risk of Burdur Province was investigated by PSHA and the results that may occur for different earthquake scenarios were evaluated.

References

[1] Gupta, I.D., The state of the art in seismic hazard analysis. *ISET Journal of Earthquake Technology*, 39, 311–346, 2002.

[2] Alpyürür, M. and Lav, M.A., An assessment of probabilistic seismic hazard for the cities in Southwest Turkey using historical and instrumental earthquake catalogs. *Natural Hazards*, 114, 1-31, 2022.

[3] Alpyürür, M. and Lav, M.A., Burdur Kent Merkezinin Deterministik Sismik Tehlike Analizi, *9.Türkiye Deprem Mühendisliği Konferansı*, İTÜ, İstanbul, 2021.

[4] Dipova, N. and Cangir, B., Probabilistic seismic hazard assessment for the two layer fault system of Antalya (SW Turkey) area. *Journal of Seismology,* 21, 1067–1077, 2017.

[5] Deniz, A, Korkmaz, K.A., Irfanoglu, A., Probabilistic seismic hazard assessment for Izmir, Turkey. *Pure and Applied Geophysics,* 167, 1475–1484, 2010.

[6] İnce, G.Ç, Yılmazoğlu M.U., Probabilistic seismic hazard assessment of Muğla, Turkey. *Natural Hazards,* 1–30, 2021.

[7] Kırım, S., Budakoğlu, E., Horasan, G., Probabilistic seismic hazard assessment for Isparta province (Turkey) and mapping based on GIS. *Arabian Journal of Geosciences,* 14, 1–15, 2021.

[8] Kutanis, M., Ulutaş, H., Işik, E., PSHA of Van province for performance assessment using spectrally matched strong ground motion records. *Journal of Earth System Science,* 127(7), 1-14, 2018.

[9] Över, S., Yilmaz, H., Pinar, A., Özden, S., Ünlügenç, U. C., Kamaci, Z., Plio-Quaternary Stress State in the Burdur Basin, SW-Turkey. *Tectonophysics,* 588, 56–68, 2013.

[10] Taymaz, T. and Price, S., The 1971 May 12 Burdur earthquake sequence, SW Turkey: a synthesis of seismological and geological observations. *Geophysical Journal International,* 108(2), 589–603, 1992.

[11] Asti, R, Faccenna, C., Rossetti, F., et al., The Gediz supradetachment system (SW Turkey): magmatism, tectonics, and sedimentation during crustal extension. *Tectonics,* 38, 1414–1440, 2019.

[12] Aktug, B., Nocquet, J.M., Cingöz, A., et al., Deformation of western Turkey from a combination of permanent and campaign GPS data: Limits to block-like behavior. *Journal of Geophysical Research: Solid Earth,* 114, 2009.

[13] Gutenberg, B. and Richter, C.F., Frequency of earthquakes in California. *Bulletin of the Seismological Society of America,* 34, 185–188, 1944.

[14] Ordaz, M., and Salgado-Gálvez, M.A., R-CRISIS validation and verification document. Technical Report. Mexico City, Mexico, 2017.

[15] Cornell, C.A. and Vanmarcke, E.H., The Major Influences on Seismic Risk. *Proceedings of the fourth world conference on earthquake engineering,* 69–83, 1969.

[16] Bayrak, Y., and Bayrak, E., An Evaluation of Earthquake Hazard Potential for Different Regions in Western Anatolia Using the Historical and Instrumental Earthquake Data. *Pure and Applied Geophysics,* 169(10), 1859–1873, 2012.

[17] Kalafat, D., Güneş, Y., Kara, M., Deniz, P., Kekovalı, K., Kuleli, H. S., Gülen, L., Yılmazer, M., Özel, N., A revised and extended earthquake catalogue for Turkey since 1900 (M≥ 4.0). Boğaziçi University, Kandilli Rasathanesi ve Deprem Araştırma Enstitüsü, Bebek-İstanbul, 553, 2007.

[18] Akkar, S., Azak, T., Çan, T., Çeken, U., Demircioğlu, M. B., Duman, T., Erdik, M., Ergintav, S., Kadirioğlu, F. T., Kalafat, D., Türkiye sismik tehlike haritasının güncellenmesi projesi.UDAP-Ç-13-06, AFAD, 2014.

[19] Reasenberg, P., Second-order moment of central California seismicity, 1969–1982. *Journal of Geophysical Research: Solid Earth,* 90(B7), 5479–5495, 1985.

[20] Wiemer, S., A software package to analyze seismicity: ZMAP. *Seismological Research Letters,* 72(3), 373–382, 2001.

[21] Aki, K., Maximum likelihood estimate of b in the formula log N= a-bM and its confidence limits. *Bull. Earthq. Res. Inst., Tokyo Univ.,* 43, 237–239, 1965.

[22] Gregori, S. D., and Christiansen, R., Seismic hazard analysis for central-western Argentina. *Geodesy and Geodynamics,* 9(1), 25–33, 2018.
[23] Yunatcı, A.A., GIS Based seismic hazard mapping of Turkey, Ph.D. thesis, Middle East Technical University, Ankara, Turkey, 2010.

[24] Abrahamson, N.A., Silva, W.J., Kamai, R., Summary of the ASK14 ground motion relation for active crustal regions. *Earthquake Spectra,* 30(3), 1025–1055, 2014.

[25] Campbell, K.W. and Bozorgnia, Y., NGA-West2 ground motion model for the average horizontal components of PGA, PGV, and 5% damped linear acceleration response spectra. *Earthquake Spectra,* 30(3), 1087–1115, 2014.

[26] Chiou, B.S.J. and Youngs, R.R., Update of the Chiou and Youngs NGA model for the average horizontal component of peak ground motion and response spectra. *Earthquake Spectra,* 30(3), 1117–1153, 2014.

[27] Boore, D.M., Stewart, J.P., Seyhan, E., Atkinson, G.M., NGA-West2 equations for predicting PGA, PGV, and 5% damped PSA for shallow crustal earthquakes. *Earthquake Spectra,* 30(3), 1057–1085, 2014.

[28] Idriss, I.M., An NGA-West2 Empirical model for estimating the horizontal spectral values generated by shallow crustal earthquakes. *Earthquake Spectra,* 30(3), 1155–1177, 2014.

[29] Akkar, S., Sandıkkaya, M.A., Bommer, J.J., Empirical ground-motion models for point- and extended-source crustal earthquake scenarios in Europe and the Middle East. *Bulletin of Earthquake Engineering,* 12(1), 359–387, 2014.

[30] Derras, B., Bard, P.Y., Cotton, F., Site-condition proxies, ground motion variability, and data-driven GMPEs: Insights from the NGA-West2 and RESORCE data sets. *Earthquake Spectra,* 32(4), 2027–2056, 2016.

[31] Cornell, C.A., Engineering seismic risk analysis. *Bulletin of the Seismological Society of America,* 58(5), 1583–1606, 1968.